arXiv:hep-ph/0007182v1 18 Jul 2000

BNL–NT–00/18
TAUP–2637–2000
July 17, 2000

QCD Instantons and the Soft Pomeron

Dmitri Kharzeev, [1,2] Yuri V. Kovchegov, [1,3] Eugene Levin [1,3]

[1] *Physics Department, Brookhaven National Laboratory*
Upton, NY 11973, USA

[2] *RIKEN–BNL Research Center, Brookhaven National Laboratory*
Upton, NY 11973, USA

[3] *HEP Department, School of Physics and Astronomy*
Tel Aviv University, Tel Aviv 69978, Israel

We study the rôle of semi–classical QCD vacuum solutions in high energy scattering by considering the instanton contribution to hadronic cross sections. We propose a new type of instanton–induced interactions ("instanton ladder") that leads to the rising with energy cross section $\sigma \sim s^{\Delta}$ of Regge type (the Pomeron). We argue that this interaction may be responsible for the structure of the soft Pomeron. The intercept $\Delta > 0$ is calculated. It has a non–analytic dependence on the strong coupling constant, allowing a non-singular continuation into the non-perturbative region. We derive the Pomeron trajectory, which appears to be approximately linear in some range of (negative) momentum transfer t, but exhibits a curvature at small t. Possible rôle of instantons in multiparticle production is also discussed.

I. INTRODUCTION

QCD vacuum is known to possess a rich structure. A striking example is provided by the existence of (Euclidean) classical solutions – instantons [1], which are responsible for non-trivial topological properties of the theory [2–4]. While the influence of instantons on the properties of hadrons and their interactions at low energies have been extensively studied [3,5,6] (for a review, see [7]), the rôle of topological effects in high energy collisions is still an open and fascinating problem [8].

In electroweak theory, significant interest was excited by the possibility of baryon number non–conservation caused by instantons at the collision energy above 10 TeV [9–14]. In QCD, the instanton contribution to the structure functions of deep–inelastic scattering was studied in Refs. [15,16], while the cross section for gluon–gluon scattering mediated by instantons was considered in Refs. [13,17–19].

Recently, it has been proposed [20] that the existence of semi–classical solutions in QCD can have important consequences also for hadron scattering at high energies, inducing a non–perturbative, and possibly dominant, contribution to the scattering amplitude. This approach was shown to lead to the "soft" pomeron with the intercept $\alpha_P - 1 \simeq 0.1$ which has a non–trivial dependence on the strong coupling and the numbers of colors and flavors [1]. The method used in that work was based on low energy theorems of broken scale invariance [22], and did not assume any specific form of the semi–classical solutions. This approach was based on the low energy theorems [22] for the trace of the QCD energy-momentum tensor taken in the chiral limit of massless quarks

$$\theta^{\mu}_{\mu} \,=\, -\frac{bg^2}{32\pi^2}\, F^{a\alpha\beta}\, F^{a}_{\alpha\beta}, \tag{1}$$

where $b = (11N_c - 2N_f)/3$ and $F^{a\alpha\beta}$ is the gluonic field strength tensor. The low energy theorems derived in [22] state that

$$i\int d^4x\,(0|T\theta^{\mu}_{\mu}(x)\theta^{\nu}_{\nu}(0)|0) \,=\, -4(0|\theta^{\mu}_{\mu}(0)|0). \tag{2}$$

Comparing Eqs. (1) and (2) one can conclude that the low energy theorem (2) can only be satisfied by a strong gluonic field [2]

$$A_{\mu} \,\sim\, \frac{1}{g}. \tag{3}$$

The strong field of Eq. (3) is usually associated with the quasi-classical solutions of QCD. This quasi-classical field has been employed in [20] to provide gluonic interactions, which, after being iterated in the t-channel gave rise to a pomeron-like behavior of the corresponding cross sections.

Here we would like to develop the idea proposed in [20] and explore the effects of quasi–classical fields on high energy scattering. Therefore, for the purpose of this paper we will consider a particular type of this classical field: we will assume that the field is given by the instanton solution [1]. We will employ instanton fields, which would allow us to quantify the assumption of the quasi–classical fields being responsible for the pomeron–like behavior of the cross sections. Nevertheless we can not rule out the possibility of some other quasi–classical gluonic fields giving a significant contribution to the processes considered below.

The instanton calculations are better justified in the electroweak theory, where the coupling is small and one can hope that quantum corrections to the classical instanton solution are small. Therefore the calculation that will be presented below can also be repeated for the electroweak interactions, where it would possibly also give a cross section that rises with energy [23] [3].

Shuryak [24] has argued that the explicit use of instantons could provide a useful way to interpret and extend the results of [20]. Very recently, Shuryak and Zahed [25] analyzed Euclidean scattering induced by the instantons, and analytically continued their results to Minkowski space using the correspondence between Euclidean angle and Minkowski rapidity [26]. Their result is a constant cross section, which does not rise with energy.

The purpose of the present paper is to investigate the effect of the instantons on the dynamics of gluon ladders in high energy scattering. Our approach here is complementary to the one taken in Ref. [20]; even though it is hindered by significant numerical uncertainties, it provides a deeper insight into the mechanism of non–perturbative effects in high energy scattering. As will become clear later, our treatment of the problem is different from Ref. [25]; while the authors of that paper consider a purely classical contribution to the scattering amplitude, we attempt at evaluating the leading quantum terms arising in perturbation theory built in the background of classical instanton fields.

The proposed mechanism of the pomeron is illustrated in Fig. 1. The pomeron is being constructed by resummation of the ladder diagrams, similarly to the well-known BFKL pomeron [27,28]. The emission vertices of our pomeron ladder are given by the multiple gluon interaction vertices generated by the instantons

---

[1] Analogous non–perturbative behavior was also established in the scattering of color dipoles at low energy [21].

[2] Unfortunately the applications of low energy theorems of Eq. (2) depends very much on the way one subtracts the perturbative contribution to the correlation functions [22]. Lattice simulations have also encountered similar problems. We thank Al Mueller for clarifying this point to us.

[3] We thank Larry McLerran for bringing our attention to this problem.

[9]. The vertices connect to two gluons in the t-channel and produce several gluons in the t-channel. We sum over all possible numbers of the produced t-channel gluons in each vertex [9,10]. The t-channel lines in the ladder of Fig. 1 will be taken as the usual gluon lines for most of our paper. In principle one should include the virtual corrections in the t-channel, which may lead to reggeization of the gluons [27,28]. We will present an estimate of these virtual corrections. However the exact calculation and the answer to the question of whether gluon reggeization happens in our case will be addressed elsewhere [29]. For most of this paper we will work in pure gluodynamics with no quarks. However, at the end of the paper we will present an estimate of the effect of inclusion of light quarks.

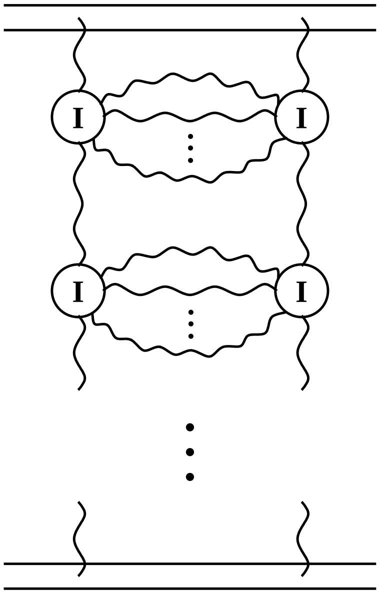

FIG. 1. The structure of soft pomeron as conjectured in the paper.

The multiple gluon vertices generated by instantons in the pomeron of Fig. 1 will be calculated in Sect. III at the classical level. The vertices include a suppression factor of $\exp\left(-\frac{2\pi}{\alpha_s}\right)$, which is due to the classical instanton action. If the coupling constant is sufficiently small ($\alpha_s \ll 1$), then this suppression factor is also small

$$\exp\left(-\frac{2\pi}{\alpha_s}\right) \ll 1 \tag{4}$$

and can be used as a parameter justifying the perturbative expansion of Fig. 1. The scale of the running coupling in this case is set by the typical size of the instantons, so that $\alpha_s = \alpha_s(1/\rho_0)$. We assume that $\alpha_s(1/\rho_0) \ll 1$, which is only marginally satisfied in QCD. Our ladder is resumming the leading logarithms of center of mass energy s, which in this case implies resummation of all powers of the parameter

$$e^{-\frac{4\pi}{\alpha_s}} \ln s \, \sim \, 1. \tag{5}$$

Note that the dependence of our small parameter on α_s is non-analytical, which will introduce the non-analytical dependence on α_s in the calculated value of the pomeron intercept.

As energy in each rung of the ladder increases, quantum corrections to the tree level calculation of the vertices become important. The quantum corrections are known to modify the energy dependence of the $2 \to n$ transition vertices [9,10,13,14]. The energy dependence of the $2 \to n$ total (summed over n) cross section is given by the following formula

$$\sigma_2(s) \, \sim \, \exp\left[\frac{1}{g^2} F\left(\frac{\sqrt{s}}{E_{sph}}\right)\right]. \tag{6}$$

Here s is the center of mass energy of the system, E_{sph} is the sphaleron energy. F is known only for the small values of its argument [14]. The lowest order term in F is given by the tree level calculations, and the quantum corrections provide higher order terms in the expansion of F [9,10,13,14]. It is also known that for a large number of gluon legs (large n) the value of the saddle point is shifted. Thus for large number of produced gluons the vertices may not be exactly the same instanton–induced vertices as for small n. This only substantiates our argument that the instanton field may not be an exact mechanism responsible for the multiple gluon interactions in the ladder of Fig. 1. There are many problems related to the determination of the function $F(\sqrt{s}/E_{sph})$ [14] and we are not going to review all of them here. We will simply point out that the growth with energy of the cross section of Eq. (6) should eventually stop due to the unitarity constraint [19]

$$\sigma < \frac{const}{s} \exp\left(-const\,\frac{2\pi}{\alpha_s}\right). \tag{7}$$

Moreover, it is possible that the discussed $2 \to n$ cross section will fall off at the energies of the two incoming gluons much higher than the sphaleron energy, since the instanton effects may not be important in that kinematic region. Assuming that this is true throughout the paper we will approximate the multi gluon interactions by the tree level calculation for the energies below the sphaleron energy and we will just put it to be zero for $\sqrt{s} > E_{sph}$. This approximation is rather crude and will be improved in the subsequent work [29], where several different behaviors of the $2 \to n$ scattering cross section will be considered. In particular we will consider the case when the unitarity limit of Eq. (7) has been reached.

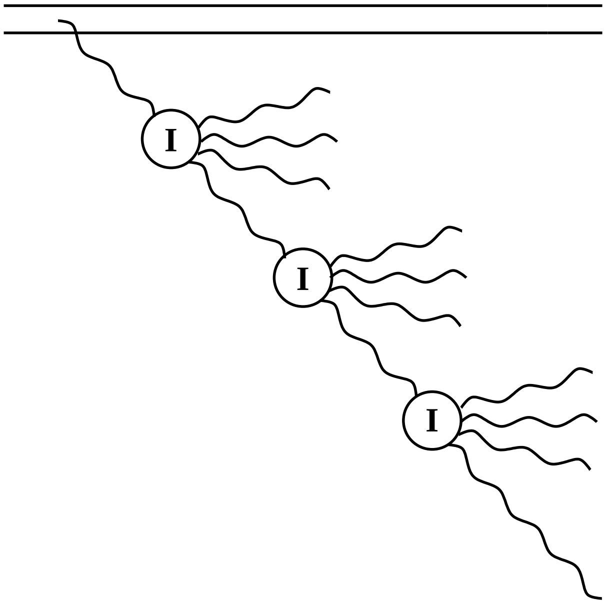

FIG. 2. Space–time picture of soft pomeron.

Let us discuss the (Minkowskian) space–time picture of high energy scattering amplitude that we are going to evaluate. Since at high energies the scattering occurs over large longitudinal distances, in order to construct the amplitude one may need to have several instantons involved in the process (see Fig. 1). At first glance, this seems to contradict the assumption of the dilute instanton gas [31] that we are going to use[4]. The resolution of this apparent problem is in the very fact that a pomeron exchange is not an instantaneous interaction. Pomeron exchange is best represented in the wave function picture of high energy interactions [30]. In that formalism in order to exchange a pomeron the colliding hadrons have to develop large multi–gluon fluctuations, which, in turn, interact with each other, which corresponds to the pomeron exchange in the usual t–channel language.

---

[4] A computation in a self–consistent instanton vacuum model would be a very interesting extension of this work.

The space–time picture of our soft pomeron constructed in the spirit of the wave function formalism is shown in Fig. 2. Single pomeron exchange corresponds to a single gluon, which, after being emitted off the original hadron, propagates through space, inducing a chain of instanton transitions between different topological vacua and producing more gluons in each transition. The coherence length of the small-x gluon in Fig. 2 is large, $\tau \sim k_+/k_\perp^2$, where k is the gluon's momentum. Thus a high energy gluon carrying a large "plus" component of momentum can propagate over large longitudinal distances inducing several instanton transitions. Even in the dilute instanton gas approximation [31] the gluon should therefore be able to generate many instanton transitions while traveling over large distances in the longitudinal direction at the given value of the impact parameter.

If the process is viewed in the rest frame of one of the hadrons, then after several instanton transitions, the propagating gluon would interact with the target hadron at rest. In the center of mass frame the propagating gluon would find another gluon coming from the second hadron and would interact with it through an instanton transition, producing more gluons.

Multiple pomeron exchanges in this picture would correspond to the case when the gluons produced in the interactions of Fig. 2 in turn start propagating through the instanton gas and interacting [32]. However, a study of that interesting scenario is beyond the scope of our paper. Here we will just argue that these multiple pomeron exchanges are suppressed compared to the single pomeron exchange contribution, for the reasons described below. Of course they will become important as the center of mass energy of the collision becomes very high.

The paper is organized as follows: after discussing the general issues related to instantons in Sect. II we will proceed to calculating the intercept of the pomeron of Fig. 1 in Sect. III. We will then calculate the slope and trajectory of the pomeron in Sect. IV and conclude by summarizing our results in Sect. V.

II. GENERAL ISSUES

In Minkowski space, instantons correspond to tunneling transitions between different topological vacua [2–4]. The instanton calculations therefore make sense only at energies much smaller than the energy of the potential barrier separating the vacua ("sphaleron" energy E_{sph}).

The BPST instanton solution in the regular gauge is given by [1]

$$A_\mu^a(x) \,=\, \frac{2\ \eta_{a\mu\nu} x_\nu}{g\,(x^2+\rho^2)}, \tag{8}$$

and the corresponding field strength is

$$(G_{\mu\nu}^a)^2 = \frac{192\ \rho^4}{g^2\,(x^2+\rho^2)^4}. \tag{9}$$

The energy along the instanton path can be defined as

$$E(\tau) = \frac{1}{8}\int d^3x\ (G_{\mu\nu}^a)^2, \tag{10}$$

and its maximum at $\tau = 0$ corresponds to the sphaleron energy (see [33]):

$$E_{sph} = E(\tau=0) = \frac{3\ \pi^2}{\rho}\ \frac{1}{g^2} = \frac{3\pi}{4\,\alpha_s\,\rho}. \tag{11}$$

To estimate this quantity, we take $\rho \simeq (700\ \mathrm{MeV})^{-1}$, and $\alpha_s(1/\rho) = g^2/4\pi \simeq 0.7$; we get $E_{sph} \simeq 2.4 \div 2.6$ GeV.

At first glance, this value of E_{sph} suggests that the perturbative treatment about the instanton solution is not applicable for hadron scattering at high energies $\sqrt{s} >> E_{sph}$. However, this conclusion is premature. Indeed, the space–time picture of high energy scattering discussed in the Introduction implies that the scattering is described by the ladder–type diagrams, where the number of rungs is proportional to rapidity $y \sim lns$, and the energy in each rung E_{rung} is independent of the total collision energy (E_{rung} is typically on the order of a few GeV [34]). The crucial condition is therefore $E_{rung} << E_{sph}$, and it is likely to be satisfied (later, we will see that this is indeed the case). Therefore, the applicability of the instanton–based approach to high energy scattering is, at least *a priori*, plausible.

Later we will find it convenient to use the singular gauge for the instanton field (the gauge in which the singularity of the potential is shifted to the origin); the corresponding expression is

$$A^a_\mu(x) \;=\; \frac{2\,\rho^2 \overline{\eta}_{a\mu\nu} x_\nu}{g\, x^2 (x^2+\rho^2)}. \tag{12}$$

In momentum space, the instanton field is given by

$$A^a_\mu(k) \;=\; \frac{i(4\pi)^2}{g}\,\frac{\overline{\eta}_{a\mu\nu}\, k_\nu}{(k^2)^2}\,\left[1-\frac{1}{2}\,(k\rho)^2\, K_2(k\rho)\right]. \tag{13}$$

III. SOFT POMERON: THE INTERCEPT

In this section we will calculate the intercept of the soft pomeron depicted in Fig. 1 to hadronic cross sections and will calculate the intercept of the soft pomeron given by that equation. We assume that the scale of the running coupling constant is being set by the typical size of the QCD instanton ρ_0, and that the coupling constant at that scale is small $\alpha_s(1/\rho_0) \ll 1$. This assumption is marginally well satisfied in QCD, but is crucial for the use of QCD instantons. In the recent year there have been proposed several scenarios of how the strong coupling constant behaves at large distances [35,36] suggesting that it never becomes larger than 1. If the ideas stated in [35,36] are correct then our small coupling assumption is likely to be justified. Otherwise we note that the small coupling assumption is of course better justified for electroweak interactions [23].

Assuming that $\alpha_s \ll 1$ we will neglect all the usual perturbative QCD vertices as bringing extra powers of α_s. We will be resumming only the instanton–induced vertices, which give powers of $\exp\left(-\frac{2\pi}{\alpha_s}\right) \ll 1$ and our model of the pomeron could be viewed as resumming powers of this parameter.

The structure of this section is the following. We will first derive the intercept of the pomeron of Fig. 1. Then we will estimate the magnitude of virtual corrections to the real emission diagrams of Fig. 1. We will then calculate the numerical value of the pomeron intercept predicted by our model.

A. Calculation of the intercept

To be able to calculate the diagrams in Fig. 1 we have to construct the basic vertex employed there — the vertex coupling several gluons to each other through an instanton. This will be done in a way similar to the calculations of the baryon number violating amplitudes involving instantons in electroweak theory done in [9]. To calculate the multiple gluon vertex we have to construct the Green function

$$G^{aba_1\ldots a_n}_{\alpha\beta\mu_1\ldots\mu_n}(q_1,q_2;k_1,\ldots,k_n) \;=\; (2\pi)^4\delta^4(q_1+q_2-k_1-\ldots-k_n)\;\left\langle\, A^a_\alpha(q_1)\,A^b_\beta(q_2)\,A^{a_1}_{\mu_1}(k_1)\,\ldots\,A^{a_n}_{\mu_n}(k_n)\,\right\rangle, \tag{14}$$

where $A^a_\mu(k)$ are instanton fields given by Eq. (13) and the brackets $\langle\ldots\rangle$ imply averaging over the instanton sizes in the single instanton sector. The Green function of Eq. (14) is depicted in Fig. 3. It combines two space-like t-channel gluons carrying momenta q_1 and q_2 with n final state gluons with momenta $k_1 \ldots k_n$, which are taken to be on the mass shell. Thus, in Minkowski space, $q_i^2 = -\underline{q}_i^2$, where $\underline{q}_i$ is the transverse component of the gluon's momentum, and $k_i^2 = 0$. We need the Green function to be in the momentum space representation because we are going to use it in the momentum space diagram calculations below. The difference between our Green function and the one usually considered in the calculations of $2 \to n$

process in QCD and electroweak theory [9,15,19] is that the two on-mass shell gluons in the initial state of the electroweak process are substituted here by two t-channel gluons which are far off mass shell.

Of course the Green function of Eq. (14) describes the multiple gluon interactions through an instanton only at not very high energies. As energy increases the quantum corrections start becoming important [13], as was discussed in the Introduction. At very high energies of the incoming pair of gluons the quantum corrections modify the behavior of the Green function and the corresponding $2 \to n$ cross section. In our approach we assume that at high center of mass energies of the hadron–hadron (or quarkonium–quarkonium) scattering the dominant contribution comes from the pomeron diagrams in Fig. 1 with a large number of rungs in the ladder. Thus the energy per rung, or, equivalently, per vertex in the ladder remains not too large, justifying the use of the Green function of Eq. (14). We will return to quantify this issue below.

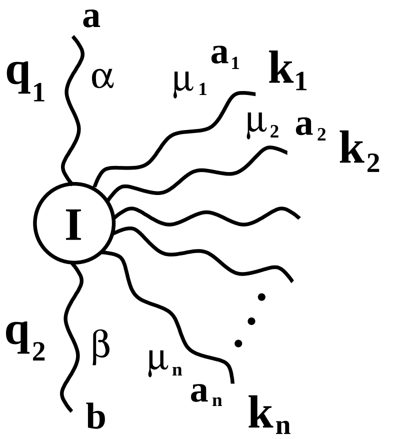

FIG. 3. The multiple gluon vertex essential for construction of soft pomeron as described in the text.

For a gluon on the mass shell the instanton field of Eq. (13) becomes

$$A^a_\mu(k) \;\to\; \frac{i4\pi^2\rho^2}{g}\,\frac{\overline{\eta}_{a\mu\nu}\,k_\nu}{k^2} \qquad \text{as} \qquad k^2 \to 0. \tag{15}$$

Substituting the field of Eq. (15) for each k_i line into Eq. (14) and employing the full instanton field of Eq. (13) for the q lines we obtain

$$G^{aba_1\ldots a_n}_{\alpha\beta\mu_1\ldots\mu_n}(q_1,q_2;k_1,\ldots,k_n) \;=\; (2\pi)^4\delta^4(q_1+q_2-k_1-\ldots-k_n)\int_0^\infty d\rho\, n(\rho)\,\rho^{2n}\left(\frac{i4\pi^2}{g}\right)^n \frac{-(4\pi)^4}{g^2}$$

$$\times\left(\prod_{i=1}^n \frac{\overline{\eta}_{a_i\mu_i\nu_i}k_{\nu_i}}{k_i^2}\right)\frac{\overline{\eta}_{a\alpha\gamma}\,q_{1\gamma}}{(q_1^2)^2}\left[1-\frac{1}{2}\,(q_1\rho)^2\,K_2(q_1\rho)\right]\frac{\overline{\eta}_{b\beta\delta}\,q_{2\delta}}{(q_2^2)^2}\left[1-\frac{1}{2}\,(q_2\rho)^2\,K_2(q_2\rho)\right], \tag{16}$$

where $n(\rho)$ is the size distribution of instantons. We want to obtain an effective vertex for multiple pomeron interactions. For that we have to truncate the external legs of the Green function of Eq. (16). To amputate the propagators of the external gluon lines one has to also remove the numerators of these propagators. For that we need to know the gauge condition of the fields of Eq. (12) and Eq. (13). Usually the field of Eq. (12) is derived using the Schwinger gauge condition $x_\mu\,A_\mu\,=\,0$. However, we note that it also satisfies the covariant gauge condition $\partial_\mu\,A_\mu\,=\,0$. Therefore we will be using it as a covariant (Feynman) gauge field and will employ it in the covariant gauge calculation of diagrams. Therefore, to truncate the Green function of Eq. (16) we have to just multiply it by $q_1^2\,q_2^2\,k_1^2\,\ldots\,k_n^2$. The resulting amputated Green function is

$$\Gamma^{aba_1\ldots a_n}_{\alpha\beta\mu_1\ldots\mu_n}(q_1,q_2;k_1,\ldots,k_n) \;=\; (2\pi)^4\delta^4(q_1+q_2-k_1-\ldots-k_n)\int_0^\infty d\rho\, n(\rho)\,\rho^{2n}\left(\frac{i4\pi^2}{g}\right)^n \frac{-(4\pi)^4}{g^2}$$

$$\times \left(\prod_{i=1}^{n} \overline{\eta}_{a_i \mu_i \nu_i} k_{\nu_i} \right) \frac{\overline{\eta}_{a\alpha\gamma}\, q_{1\gamma}}{q_1^2} \left[1 - \frac{1}{2}\, (q_1 \rho)^2\, K_2(q_1\rho) \right] \frac{\overline{\eta}_{b\beta\delta}\, q_{2\delta}}{q_2^2} \left[1 - \frac{1}{2}\, (q_2 \rho)^2\, K_2(q_2\rho) \right]. \qquad (17)$$

Now we are in the position to calculate the intercept of the soft pomeron in Fig. 1. The calculation will be done in the Minkowski space. To perform it we have to first multiply the amputated Green function of Eq. (17) by the numerators of the propagators of the t-channel gluons in the light cone gauge (Weizsäcker–Williams approximation)

$$\frac{q_{1\alpha}^{\perp}}{q_{1+}}\, \frac{q_{2\beta}^{\perp}}{q_{2-}},$$

where the gluon q_1 carries a large + component of the light cone momentum and the gluon q_2 carries a large − component. This is a standard procedure, which is described in [37] in greater detail. Then we should multiply the gluon line factors k_i's in Eq. (17) by the polarization vectors $\epsilon_i^{\lambda_i}(k_i)$ and square the amputated Green function of Eq. (17) excluding the δ function. We should keep in mind that the color space orientation of the instanton in the complex conjugate amplitude is, in principle, different from the color space orientation of the instanton in the amplitude [11,12,15,18,19]. Therefore we will have to average over all possible orientations, for which we will be using the approximation introduced in [19]. We will integrate the obtained expression over the phase space of the produced gluons and sum over colors and polarizations λ_i

$$\frac{1}{n!} \prod_{i=1}^{n} \frac{d^3 k_i}{2(2\pi)^3 \omega_i} \sum_{\lambda_i}$$

where $\omega_i = k_4^i$ and sum over n runs from 1 to infinity. We also have to multiply everything by one of each of the denominators of the propagators of the t-channel gluons [37]

$$\frac{1}{\underline{q}_1^2}\, \frac{1}{\underline{q}_2^2}$$

and average over the colors of gluons q_1 and q_2, which would give a factor of $1/(N_c^2-1)^2$. We also have to include the symmetry factor of $(n!)^2$. We end up with the following expression for the kernel of the integral equation describing the pomeron of Fig. 1

$$K(q_1^{\perp}, q_2^{\perp})\, \ln\frac{1}{x} \;=\; \frac{1}{(N_c^2-1)^2} \sum_{n=1}^{\infty} \int d^4 q\, \delta^4(q - \sum_{i=1}^{n} k_i)\, n!$$

$$\times \left(\prod_{i=1}^{n} \frac{d^3 k_i}{2(2\pi)^3 \omega_i} \int d\xi \sum_{\lambda_i} \left[\overline{\eta}_{a_i\mu_i\nu_i} k_{\nu_i}\, \epsilon_{\mu_i}^{\lambda_i}(k_i) \right] \left[U^{a_i b_i}(\xi)\, \overline{\eta}_{b_i \mu_i \nu_i} k_{\nu_i}\, \epsilon_{\mu_i}^{\lambda_i}(k_i) \right]^* \right)$$

$$\times \left(\frac{4\pi^2}{g} \right)^{2n} \frac{(4\pi)^8}{g^4}\, \frac{1}{\underline{q}_1^2\, \underline{q}_2^2} \left[\frac{\overline{\eta}_{a\alpha-}\, q_{1\alpha}^{\perp}\, \overline{\eta}_{b\beta+} q_{2\beta}^{\perp}}{\underline{q}_1^2\, \underline{q}_2^2} \right] \left[\frac{U^{aa'}(\xi)\, \overline{\eta}_{a'\alpha-}\, q_{1\alpha}^{\perp}\, U^{bb'}(\xi)\, \overline{\eta}_{b'\beta+} q_{2\beta}^{\perp}}{\underline{q}_1^2\, \underline{q}_2^2} \right]^*$$

$$\times \left[\int_0^{\infty} d\rho\, n(\rho)\, \rho^{2n} \left(1 - \frac{1}{2}\, (q_1^{\perp}\rho)^2\, K_2(q_1^{\perp}\rho) \right) \left(1 - \frac{1}{2}\, (q_2^{\perp}\rho)^2\, K_2(q_2^{\perp}\rho) \right) \right]^2, \qquad (18)$$

with $q = q_1 + q_2$. $U^{ab}(\xi)$ is the matrix of global $SU(2)$ rotations in the adjoint representation and it is responsible for rotating the instanton in the complex conjugate amplitude in the color space [11,19]. We can perform the summation over polarizations and averaging over the color space orientations of the instantons using the approximation outlined in [19]

$$\int d\xi \prod_{i=1}^{n} \sum_{\lambda_i} \left[\overline{\eta}_{a_i\mu_i\nu_i}\, k_{\nu_i}\, \epsilon^{\lambda_i}_{\mu_i}(k_i)\right] \left[U^{a_i b_i}(\xi)\overline{\eta}_{b_i\mu_i\nu_i}\, k_{\nu_i}\, \epsilon^{\lambda_i}_{\mu_i}(k_i)\right]^* \approx \left(\frac{E_{sph}^2}{3n^2}\right)^n \approx \frac{2\,\pi\, n\, E_{sph}^{2n}}{3^n\, e^{2n}\,(n!)^2} \tag{19}$$

for large n. Eq. (19) can be understood in the rest frame of the system of two t-channel gluons. There the dominant contribution to Eq. (19) comes from equally distributing center of mass energy among n final state gluons, which leads to the $(E_{sph}^2/n^2)^n$ in Eq. (19). The estimate of Eq. (19) is somewhat crude, but was justified in [15,18,19]. In writing Eq. (19) in the approximation outlined in [19] we are likely to omit factors of n. However, as could be seen from the calculations below, we do not have the precision to keep all the powers of n at this point. Extra powers of n may arise from different ways of averaging over the instanton sizes (see Eq. (29) and Eq. (35)). The q^2 integration in Eq. (18) is sharply peaked at the upper cutoff, as will be seen from the calculations presented below, which we will put to be E_{sph}. This allowed us to just put E_{sph}^2 in Eq. (19). However, the uncertainty in our knowledge of E_{sph}^2 may also introduce significant numerical changes, which we can not control at the moment. We are going to clarify those in the subsequent work [29]. We have also put $U^{ab}(\xi) = 1$ for the t-channel gluon lines. As the left hand side of Eq. (19) should of course be a Lorentz invariant expression in Minkowski space it can only depend on boost invariant quantities. Thus we can see that for $n = 1$ the answer should be proportional to $k^2 = 0$ and should, therefore, be zero. For higher values of n the left hand side of Eq. (19) may depend on the products of momenta of different gluons, which results in a non-zero answer.

In evaluating the expression in Eq. (18) we have to note that the perturbative size distribution of the QCD instantons $n(\rho)$ is divergent at large sizes ρ. However, the lattice data [16] suggests that the distribution actually starts to fall off very steeply with increasing ρ after some critical value of $\rho = \rho_0$. This behavior could be expected by the following argument based on the low energy theorem of Eq. (2), which has become known as "$b/4$" problem [6,7,38,39]. The issue is the following: it is impossible to satisfy the low energy theorem of Eq. (2) with a purely classical field. The energy-momentum tensor of a classical field given by Eq. (1) has only one power of b in it, since the classical field has no information about renormalization and running coupling constant in it. Thus if one tries to satisfy Eq. (2) with this energy momentum tensor one would get an extra power of b on the left hand side which would not cancel. The commonly accepted resolution of this problem is to assume that the instantons in the instanton gas interact with each other, which leads to a different infrared cutoff on the integrals over ρ on the left and right hand sides of Eq. (2) [38]. This leads us to conclude that QCD regularizes itself at large distances by cutting off the growth of the instanton size distribution through some non-perturbative, but not classical mechanism. This conclusion seems to be supported by lattice data [16]. For the purpose of this paper, in order to cure the problem we have to introduce an upper cutoff ρ_0 in the ρ integrals in Eq. (18).

In our approximation the sum over polarizations and colors (Eq. (19)) became independent of k_i's. Therefore we can perform the integration over the phase space of n gluons. The integration yields

$$\delta^4(q - \sum_{i=1}^{n} k_i) \prod_{i=1}^{n} \frac{d^3k_i}{2\omega_i} = \frac{(\pi/2)^{n-1}(q^2)^{n-2}}{(n-1)!\,(n-2)!}. \tag{20}$$

After some simple algebra Eq. (18) becomes

$$K(q_1^\perp, q_2^\perp)\, \ln\frac{1}{x} = \frac{1}{(N_c^2-1)^2} \sum_{n=2}^{\infty} \int d^2\underline{q}\, \frac{dq_+}{2\,q_+}\, dq^2\, n!\, \frac{1}{(2\pi)^{3n}}\, \frac{(\pi/2)^{n-1}(q^2)^{n-2}}{(n-1)!\,(n-2)!}\, \frac{2\,\pi\, n\, E_{sph}^{2n}}{3^n\, e^{2n}\,(n!)^2} \left(\frac{4\pi^2}{g}\right)^{2n}$$

$$\times \frac{(4\pi)^8}{g^4}\, \frac{1}{q_{1\perp}^4\, q_{2\perp}^4} \left[\int_0^{\rho_0} d\rho\, n(\rho)\, \rho^{2n} \left(1 - \frac{1}{2}\,(q_1^\perp\rho)^2\, K_2(q_1^\perp\rho)\right) \left(1 - \frac{1}{2}\,(q_2^\perp\rho)^2\, K_2(q_2^\perp\rho)\right)\right]^2. \tag{21}$$

We note again that the instanton size distribution is very sharply peaked around its' maximum given by ρ_0. This statement is supported by the lattice data [16] and by various instanton models [31]. The size distribution for $\rho < \rho_0$ is very close to the perturbative results [16,40], which sharply increases near ρ_0. For $\rho > \rho_0$ the distribution falls off steeply [16], justifying our cutoff procedure in Eq. (21). Thus without loosing the accuracy of our calculations we can put $\rho = \rho_0$ in the factors containing the confluent Bessel functions in Eq. (21). Now we can see that the transverse momentum integration factorizes in the expression for the kernel of the equation for the pomeron–mediated forward amplitude (21). Each segment of the ladder in Fig. 1, consisting of the square of the Green function of Fig. 3, gives a factor of

$$K(q^{\perp}) \;\equiv\; \frac{1}{q_{\perp}^4}\left(1-\frac{1}{2}\,(q_{\perp}\rho_0)^2\,K_2(q_{\perp}\rho_0)\right)^2 \tag{22}$$

to the rung of the ladder above it and a similar factor (with a different momentum) to the rung below it. Therefore each rung of the ladder brings in a square of the factor in Eq. (22) integrated over the transverse momentum

$$I_0\,\rho_0^6 \;=\; \int d^2q_{\perp}\,\frac{1}{q_{\perp}^8}\,\left(1-\frac{1}{2}\,(q_{\perp}\rho_0)^2\,K_2(q_{\perp}\rho_0)\right)^4 . \tag{23}$$

Therefore, to obtain the pomeron's intercept out of the integral kernel in Eq. (21) we should substitute the integral I_0 instead of the transverse momentum integration in Eq. (21). I_0 is easy to evaluate numerically, which gives

$$I_0 \;\approx\; 0.014. \tag{24}$$

Integration over q_+ in Eq. (21) gives a factor of $\ln\frac{1}{x}$. Actually, the summation of the diagrams in Fig. 1 can be performed by the following simple integral equation

$$\phi(q_1^{\perp}, Y=\ln(1/x)) \;=\; K(q_1^{\perp}) \;+\; CK(q_1^{\perp})\int_0^Y dy\int d^2q_2^{\perp}\,K(q_2^{\perp})\,\phi(q_2^{\perp}, y) \tag{25}$$

where the kernel of Eq. (21) is $K(q_1^{\perp}, q_2^{\perp}) = CK(q_1^{\perp})\cdot K(q_2^{\perp})$ and constant C absorbs sum over n and integral over q^2 in Eq. (21). $\phi(q^{\perp}, Y=\ln(1/x))$ denotes the sum of all diagrams of Fig. 1–type, i. e., the pomeron–induced structure function or cross section. The initial condition is given by $K(q_1^{\perp})$, which is not crucial for us and convenient for determination of the intercept. One can check that

$$\phi(q^{\perp}, Y) = K(q^{\perp})\cdot\exp(\Delta_{soft}\,Y) \tag{26}$$

is the solution of Eq. (25) with

$$\Delta_{soft} \;=\; C\int d^2q^{\perp}\;K^2(q^{\perp})\;. \tag{27}$$

A much more serious problem is posed by the integration over q^2 and summation over n (both absorbed in C in Eq. (25)) in Eq. (21), which is potentially very dangerous if one allows the upper limit of the integration to be as large as the center of mass energy of the system. This is what Eq. (21) seems to suggest if one takes it at face value. However, our Eq. (21) is valid only at relatively low energies. As energy increases quantum corrections become important. As was shown in [17] the instanton-induced cross section for 2 → n process in QCD falls off with energy for energies above certain threshold energy E_0 due to quantum correction calculated in [13]. Similar behavior results from the unitarity constraint derived in [19]. Here we assume that this is also the case for our expression for the intercept. Namely we believe that at higher energies per rung in the ladder the quantum corrections would significantly slow down and later on completely overturn the growth of the expression in Eq. (21) with energy, as was discussed in the Introduction. These effects could be taken into account by putting an effective upper cutoff E_{sph}^2 in the q^2 integration in Eq. (21). After performing all the integrations mentioned above Eq. (21) yields the following expression for the pomeron's intercept

$$\Delta_{soft} \;=\; \frac{\pi\,I_0\,\rho_0^4}{(N_c^2-1)^2}\,\frac{(4\pi)^6}{\alpha^3}\,\frac{E_{sph}^2\,\rho_0^2}{6\,e^2}\,\sum_{n=2}^{\infty}\frac{1}{[(n-1)!]^3}\left(\frac{\pi\,E_{sph}^4}{6\,\alpha\,e^2}\right)^{n-1}\left(\int_0^{\rho_0} d\rho\,n(\rho)\,\rho^{2n}\right)^2 . \tag{28}$$

Employing the same argument about the sharpness of the distribution of $n(\rho)$ [16] as was used in performing the transverse momentum integral in Eq. (21) we could rewrite

$$\int_0^{\rho_0} d\rho\, n(\rho)\, \rho^{2n} \;\approx\; \rho_0^{2n}\, N_0, \tag{29}$$

where we have defined

$$N_0 \;=\; \int_0^{\rho_0} d\rho\, n(\rho). \tag{30}$$

Substituting Eq. (29) into Eq. (28) we obtain

$$\Delta_{soft} \;=\; \frac{\pi\, I_0\, (N_0 \rho_0^4)^2}{(N_c^2-1)^2}\, \frac{(4\pi)^6}{\alpha^3}\, \frac{E_{sph}^2\, \rho_0^2}{6\, e^2} \sum_{n=2}^{\infty} \frac{1}{[(n-1)!]^3} \left(\frac{\pi\, E_{sph}^4\, \rho_0^4}{6\, \alpha\, e^2}\right)^{n-1}. \tag{31}$$

Note that N_0 has the dimensions of M^{-4} and, therefore, Eq. (31) is, of course, dimensionless. We can rewrite Eq. (31) in a more compact form with the help of a generalized hypergeometric function

$$\Delta_{soft} \;=\; \frac{\pi\, I_0\, (N_0 \rho_0^4)^2}{(N_c^2-1)^2}\, \frac{(4\pi)^6}{\alpha^3}\, \frac{E_{sph}^2\, \rho_0^2}{6\, e^2} \left[{}_0F_2\left(-;1,1;\frac{\pi\, E_{sph}^4\, \rho_0^4}{6\, \alpha\, e^2}\right) - 1 \right]. \tag{32}$$

One could be a little more careful in evaluating Eq. (28). We can use the perturbative expression for the size distribution of instantons [7,40]

$$n(\rho) \;=\; d\, \frac{1}{\rho^5} \left(\frac{2\pi}{\alpha}\right)^{2N_c} e^{-\frac{2\pi}{\alpha}} \left(\frac{\rho}{\rho_0}\right)^b, \tag{33}$$

where d is given by

$$d \;=\; \frac{0.466 e^{-1.679 N_c}}{(N_c-1)!(N_c-2)!} \;\approx\; 1.5\, 10^{-3} \qquad \text{for} \qquad N_c = 3 \tag{34}$$

and $b \;=\; (11/3)\, N_c$ for pure gluodynamics. We also used $1/\rho_0$ as a renormalization scale in Eq. (33). With the distribution of Eq. (33) we obtain

$$\int_0^{\rho_0} d\rho\, n(\rho)\, \rho^{2n} \;=\; d \left(\frac{2\pi}{\alpha}\right)^{2N_c} e^{-\frac{2\pi}{\alpha}}\, \frac{\rho_0^{2n-4}}{2n+b-4}, \tag{35}$$

which, after plugging it into Eq. (28) and summation over n in it yields the following expression for the soft pomeron's intercept

$$\Delta_{soft} \;=\; \frac{\pi\, I_0\, d^2}{(N_c^2-1)^2} \left(\frac{2\pi}{\alpha}\right)^{4N_c} e^{-\frac{4\pi}{\alpha}}\, \frac{(4\pi)^6}{\alpha^3}\, \frac{1}{81}\, \frac{E_{sph}^2\, \rho_0^2}{6\, e^2} \left[{}_2F_4\left(\frac{9}{2},\frac{9}{2};1,1,\frac{11}{2},\frac{11}{2};\frac{\pi\, E_{sph}^4\, \rho_0^4}{6\, \alpha\, e^2}\right) - 1 \right], \tag{36}$$

where we have explicitly used $b = 11$ for $N_c = 3$. The perturbative instanton size distribution of Eq. (33) has been shown to fit very well the recent lattice data for $\rho \;<\; \rho_0$ [16]. Therefore the estimate of the intercept given in Eq. (36) is probably more precise than the estimate from Eq. (32). Though in both cases we have to make the same assumptions to simplify the transverse momentum integration in Eq. (21). We also had to put a cutoff on ρ integration in arriving to both Eqs. (32) and (36), which is not a very bad approximation judging from lattice data [16], but still is an approximation. In Sect. IIIC we will compare numerical predictions of Eq. (32) and Eq. (36) for the soft pomeron's intercept.

It should be stressed that the approach developed here in Eq. (25) – Eq. (36) is an example of the multiperipheral approach (see Ref. [34] and references therein). It gives all typical properties of the multiperipheral "ladder" diagrams, namely, the typical transverse momentum of produced particles (gluons) which does not depend on the total energy ($q^{\perp}\rho_0 \;\approx 2 \div 3$ in our case, which follows from Eq. (22)) and the average energy $\hat{s}$ between the produced two bunches of gluons in Fig. 1 which also does not depend on the total energy and is equal to

$$\Delta_{soft}\, \cdot\, \ln(\hat{s}/E_{sph}^2) \;\sim\; 1\;. \tag{37}$$

These features of our approach cannot be spoiled by virtual corrections but, of course, they have to be taken into account when one considers the numerical value of the pomeron intercept.

B. Virtual corrections

There are two types of virtual contributions to the soft pomeron we are discussing. One is the additional gluon exchanges between instantons in t-channel, an example of which is shown in Fig. 4B. These corrections do not introduce extra logarithms of energy ($\ln \frac{1}{x}$) in the problem. The other type of virtual contributions could come from reggeization of the gluon propagator due to the instanton interactions. This effects of course may introduce additional powers of $\ln \frac{1}{x}$.

Let us first concentrate on the corrections brought in by the t-channel gluons as demonstrated in Fig. 4B. We are going to compare the contribution of the real diagram which is included in our model of the soft pomeron above, given by Fig. 4A to the contribution of the same diagram with a virtual correction added to it, which is depicted in Fig. 4B.

The difference between the graphs in Figs. 4A and 4B is just in extra gluon line, which introduces a loop integral. After some simple algebra one can see that the integral brings in a factor

$$K \,=\, \left(\frac{4\pi^2}{g}\right)^2 \int \frac{d^4k}{(2\pi)^4} \, \frac{\left[1-\frac{1}{2}\,(k\rho_0)^2\,K_2(k\rho_0)\right]^2\,\left[1-\frac{1}{2}\,(|p-k|\rho_0)^2\,K_2(|p-k|\rho_0)\right]^2}{(k^2)^2\,[(p-k)^2]^2}, \tag{38}$$

where the labeling of the momenta is explained in Fig. 5. One of the t-channel virtual lines carries the 4-momentum k and the other one carries $p-k$. In Eq. (38) we included only the factors which make the contribution of the diagram in Fig. 4B different from the contribution of the graph in Fig. 4A. We also assumed that the instantons in the amplitude and in the complex conjugate amplitude have the same orientation in the color space. This assumption is not going to change our final answer by a large factor, and, therefore is good for the estimate we are going to perform here.

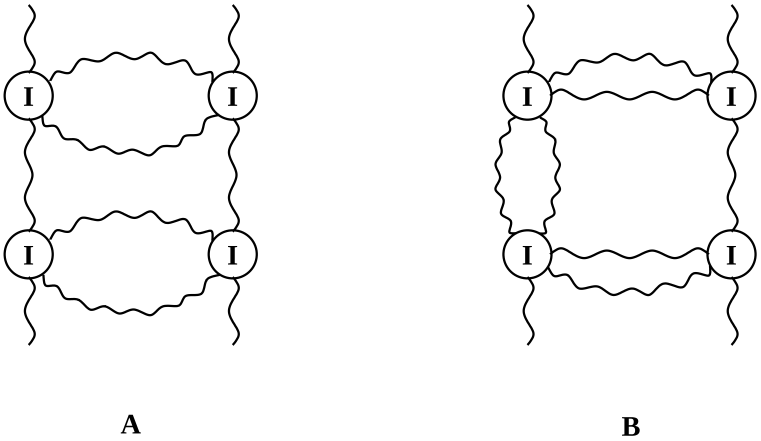

FIG. 4. (A) A "real" diagram contributing to the pomeron intercept calculated in Sect. IIIA; (B) An example of a virtual correction.

The value of the integral in Eq. (38) is easy to estimate. First we note that the expression in Eq. (38) is a decreasing function of p. Therefore one can obtain an upper bound on the value of the integral (38) by estimating it numerically for $p=0$. The result reads

$$K \,=\, 0.0052\,\frac{\pi}{2\,\alpha}\,\rho_0^4. \tag{39}$$

We have to compare the factor given by Eq. (39) to the factor given by the p-line in Fig. 4A, which is just $1/(p^2)^2$. For the estimate we can assume that approximately $p \approx 1/\rho_0$ (see Eq. (22)). Therefore we conclude that the diagram in Fig. 4B is different from the diagram in Fig. 4A by the factor of $0.0052\,\pi/2\,\alpha$. For the values of α taken at the scale corresponding to the instanton size ($\alpha(1/\rho_0) \approx 0.6$) this number is still very small, of the order of 0.01. We can see that resummation of t-channel virtual corrections, which are not enhanced by logarithms of energy can not give us a large contribution and could be neglected.

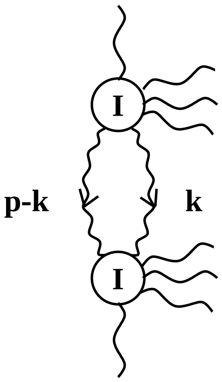

FIG. 5. Virtual diagram of Fig. 4B, which contribution is calculated in the text.

One might think that the diagram of Fig. 5 taken without the s-channel gluon lines would give us a contribution to the mass of a gluon, thereby creating a non-zero gluon's mass. However, in constructing Eq. (38) we did not impose the condition that the gluons forming the gluon loop should be in the color octet state, as one should do in calculating the correction for the gluon's mass. That condition was not used since with the s-channel gluons present in Fig. 5 the color of the pair of t-channel gluons is not fixed. Now we have to point out that for $p = 0$ the contribution of this diagram without the s-channel gluons is zero, which could be seen after projecting the t-channel gluons onto the color octet state.

The second type of virtual corrections are enhanced by the factors of $\ln\frac{1}{x}$ and are similar to gluon reggeization corrections for the BFKL pomeron [27,28]. To include these corrections which bring in the evolution in $\ln\frac{1}{x}$ one has to calculate the intercept of the same pomeron ladder of the type shown in Fig. 1 with two t-channel gluons forming a color octet combination and with the non-zero momentum transfer in the ladder. The two gluons in the t-channel should in turn include all the virtual corrections in them. A careful inclusion of the gluon reggeization proved to be a very complicated task and will be completed elsewhere [29]. here we are going to estimate these corrections.

Let us calculate the contribution of a single rung in the ladder of Fig. 1, with the ladder taken in the octet state with non-zero momentum transfer $t = -\underline{q}^2$ (see also Fig. 7). A direct repetition of calculations in section IIIA leads to the following expression for the octet channel integral $I_8(q^2)$ which replaces integral I_0 in Eq. (32) and Eq. (36) for the intercept of the Pomeron.

$$I_8(q^2)\,\rho_0^6 \;=\; \int d^2k_\perp\, \frac{|\left(\underline{k}-\frac{1}{2}\underline{q}\right)\times\left(\underline{k}+\frac{1}{2}\underline{q}\right)|^2}{[(\underline{k}+\frac{1}{2}\underline{q})^2]^3\,[(\underline{k}-\frac{1}{2}\underline{q})^2]^3}\left[1-\frac{1}{2}\left(\underline{k}+\frac{1}{2}\underline{q}\right)^2\rho_0^2\,K_2\left(|\underline{k}+\frac{1}{2}\underline{q}|\rho_0\right)\right]^2$$

$$\times\left[1-\frac{1}{2}\left(\underline{k}-\frac{1}{2}\underline{q}\right)^2\rho_0^2\,K_2\left(|\underline{k}-\frac{1}{2}\underline{q}|\rho_0\right)\right]^2, \tag{40}$$

We will now assume that the virtual corrections to our pomeron lead to reggeization of the t-channel gluons. Moreover, to estimate the trajectory we will assume that the expression for the gluon Regge trajectory has a form

$$\alpha_G(q^2) \;=\; 1 \;+\; \Delta_{soft}\,\frac{I_8(q^2)}{I_0}\;. \tag{41}$$

Eq. (41) is our estimate of the gluon's trajectory. One can see that $I_8(q^2) \to 0$ at $q^2 \to 0$.

To simplify the expression for the gluon's Regge trajectory we note that approximately

$$\frac{1}{z^4}\left[1-\frac{1}{2}\,z^2\,K_2(z)\right]^2 \;\approx\; \frac{e^{-z^2/2}}{16}. \tag{42}$$

Using Eq. (42) we can easily calculate function $I_8(q^2)$, namely, it turns out that

$$I_8(q^2) \;=\; \frac{\pi}{256}\left\{2\left(e^{-\frac{q^2\rho_0^2}{4}} \;-\; e^{-\frac{q^2\rho_0^2}{2}}\right) \;+\; \frac{q^2\rho_0^2}{2}\left[Ei\left(-\frac{q^2\rho_0^2}{4}\right) \;-\; 2\,Ei\left(-\frac{q^2\rho_0^2}{2}\right)\right]\right\}\,. \tag{43}$$

Eq. (43) should be substituted into Eq. (41) to obtain our approximation for the gluon's Regge trajectory.

Now we have to determine whether the reggeization corrections can significantly influence the value of the our pomeron's intercept. It turns out that gluon reggeization can change the value of Δ_{soft} since it leads to an additional factor in Eq. (23), which reduces this equation to the form

$$I_0\,\rho_0^6 \;=\; \int d^2q_\perp\,\frac{1}{q_\perp^8}\left(1-\frac{1}{2}\,(q_\perp\rho_0)^2\,K_2(q_\perp\rho_0)\right)^4 \;\cdot\; e^{-2\,[\alpha_G(q_\perp^2)-1]\,\ln(\hat{s}/E_{sph}^2)}\;, \tag{44}$$

where $\hat{s}$ is the energy in one rung of the ladder (see above). As we have discussed the dominant contribution in the integral of Eq. (23) comes from $q^2\rho_0^2 \approx 2-3$ (see Eq. (42)) where $2\,[\alpha_G(q_\perp^2 = 2/\rho_0^2)-1]\,\ln(\hat{s}/E_{sph}^2) \approx 0.4 \div 0.5$, since $\ln(\hat{s}/E_{sph}^2) \sim 1/\Delta_{soft}$ (see Eq. (37)). Therefore, the additional form factor in Eq. (44) due to gluon reggeization can suppress the value of I_0, and, consequently, the value of Δ_{soft} by a factor of 2 $\div$ 3. Explicit numerical calculations confirm these expectations. A more careful analysis of the contribution of virtual corrections will be done later [29]. In the numerical estimates which will be done below we have to keep in mind that virtual corrections can introduce a factor of 2 $\div$ 3 uncertainty in the value of the pomeron's intercept.

C. Value of the intercept

The main purpose of this paper is to provide a qualitative mechanism which could account for the effect of the soft pomeron. This was done in Sect. IIIA. Nevertheless, we could try to estimate the numerical value of the soft pomeron intercept obtained in Eqs. (32) and (36) and check how it compares with the experimental value of 0.08 [41].

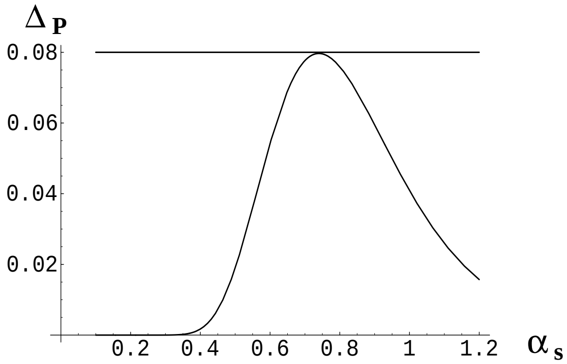

FIG. 6. Intercept of our soft pomeron as a function of α_s for $E_{sph} = 2.4\,\mathrm{GeV}$, $\rho_0 = 0.3 fm$ and the virtual corrections giving a factor of $\delta = 0.31$ suppression. The horizontal line corresponds to the phenomenological pomeron intercept [41].

At the same time one has to be very careful with the numerical estimates of the intercept in Eq. (32) and Eq. (36). It is important to realize that the intercept of Eq. (32) strongly depends on the position of the maximum of the instanton size distribution ρ_0 and on the value of the integral of this distribution over all ρ's given by N_0. The value of the intercept in Eq. (36) depends on the parameter ρ_0 since it determines the scale of the strong coupling constant. The current knowledge of these parameters is poor [16,17,42,43]. The value of N_0 seems to be undetermined up to an order of magnitude [42]. Uncertainty in the value of ρ_0 brings in an uncertainty in the value of the strong coupling constant $\alpha(1/\rho_0)$. Finally a very important question concerns the value of the cutoff, which was taken to be E_{sph} in Eqs. (32) and (36). The cutoff corresponds the maximum invariant mass of the particles produced in each vertex. In electroweak physics it correspond to the energies when the growth of the cross section of the $2 \to n$ instanton-induced process slows down and, maybe, even starts decaying. In QCD it may correspond to the energy at which the unitarity limit of the $2 \to n$ process is reached [19]. The exact value of the energy at which this happens is still not determined precisely [13,11,12,17,19]. It is one of the most crucial assumptions of this work that the turnover of the cross section does happen in QCD and that the corresponding invariant mass E_{sph}^2 is not too large.

The intercept of the pomeron calculated above (Eq. (36)) has been derived for pure gluodynamics. If we want to compare our result to the experimentally measured one [41] we have to include quarks in the theory. They would introduce suppression of the amplitudes through the Faddeev–Popov determinant [2]. Quark lines could be included in the scattering in two ways: they could be produced from an instanton into the final state, in which case the suppression factor they introduce is small, of the order of 10^{-5}, so this type of quark effects could be neglected. Alternatively the quarks could be absorbed in the gluon condensate [44]. In the latter case the suppression factor in the distribution of instantons Eq. (33) is [44]

$$\prod_{q=u,d,s,\ldots} 1.3 \left(m_q\,\rho - \frac{2\pi^2}{3}\,(0|\overline{q}q|0)\,\rho^3 \right). \tag{45}$$

The suppression for the intercept of Eq. (36) is given by the square of the factor in Eq. (45). For our estimate we will just put $\rho = \rho_0$ in Eq. (45) and use $(0|\overline{q}q|0) = -(0.25\,\mathrm{GeV})^3$. Taking the product over three flavors we obtain a suppression factor of 0.023 for the intercept.

Keeping in mind all of the above mentioned limitations we substitute the value of $E_{sph} = 2.4\,\mathrm{GeV}$ and $\rho_0 = 0.3 fm$ from [43] into Eq. (36) and plot the resulting value of the pomeron's intercept as a function of the coupling constant α_s. We also included suppression introduced by virtual corrections by including an extra factor δ on the right hand side of Eq. (36). The resulting pomeron's intercept is related to the intercept of Eq. (36) by the following relation

$$\Delta_P \,=\, \delta \left[\prod_{q=u,d,s,\ldots} 1.3 \left(m_q\,\rho_0 - \frac{2\pi^2}{3}\,(0|\overline{q}q|0)\,\rho_0^3 \right) \right]^2 \Delta_{soft} \tag{46}$$

In the plot shown in Fig. 6 we have put $\delta = 0.31$. Of course we have to admit that the plot in Fig. 6 depends on the value of the suppression factor δ. It is also very sensitive to the cutoff E_{sph}. A work on putting some constraints on these parameters is under way [29]. With the progress in the field of instanton models the exact numerical value of the soft pomeron intercept might be calculated with more confidence and precision.

The maximum of the intercept depicted in Fig. 6 is close to the experimental result of 0.08, shown there by a horizontal line. The value of the coupling constant at the scale set by the instanton size ρ_0 is near the point on the plot of Fig. 6 where the maximum is achieved. Thus our value of the intercept should be about 0.08. Also, the pomeron's intercept seems to vanish at small distances (large momenta), in agreement with experimental data [41]. Also our model of soft pomeron allows a non-singular continuation of the value of the intercept into the region of large distances and large coupling constant. Even if the strong coupling constant becomes very large at small momenta (large distances) the intercept of our pomeron still remains small (see Fig. 6). That way the strong interactions are able to yield us with a small pomeron's intercept even in the kinematic region where they are very strong. Here we have to recall that strictly speaking our quasi–classical approach is applicable only when the coupling constant is small. Nevertheless, the smallness of the intercept at large coupling is an interesting result, supported by phenomenological observations [41].

IV. SOFT POMERON: THE SLOPE AND TRAJECTORY

In this Section we are going to calculate the slope and the intercept of the soft pomeron conjectured above. We will include contribution of the virtual corrections by putting a factor δ in the expression for pomeron's trajectory (see Sect. IIIB). The quark contribution will also be treated similarly to Sect. IIIC. Therefore the slope and trajectory of the soft pomeron which will be derived below will result only from the real emissions part of its kernel. This will correspond to summing the diagrams of the type shown in Fig. 1.

To calculate the slope of the pomeron considered here we will follow the standard procedure. Let us consider a pomeron with non-zero momentum transfer described by Mandelstam variable t. A rung of the off-forward pomeron's ladder is shown in Fig. 7. One t-channel gluon carries a momentum $k + \frac{1}{2}q$, whereas the other one carries momentum $k - \frac{1}{2}q$. Thus the momentum transfer is $t = -\underline{q}^2$.

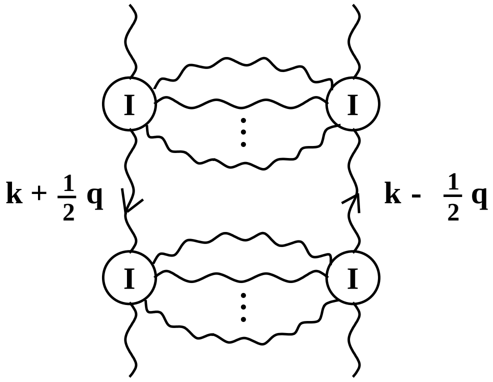

FIG. 7. Soft pomeron with non-zero momentum transfer.

It is easy to see that the only difference between the pomeron ladder with non-zero momentum transfer and the $t = 0$ pomeron considered in Sect. III is in the transverse momentum integral. An easy calculation shows that for off-forward pomeron the integral I_0 in the expression for the forward pomeron intercept (36) should be replaced by

$$I(q^2)\,\rho_0^6 \;=\; \int d^2k_\perp \, \frac{(\underline{k}^2 - \frac{1}{4}\underline{q}^2)^2}{[(\underline{k}+\frac{1}{2}\underline{q})^2]^3\,[(\underline{k}-\frac{1}{2}\underline{q})^2]^3} \left[1 - \frac{1}{2}\left(\underline{k} + \frac{1}{2}\underline{q}\right)^2 \rho_0^2\, K_2\left(|\underline{k} + \frac{1}{2}\underline{q}|\rho_0\right)\right]^2$$

$$\times \left[1 - \frac{1}{2}\left(\underline{k} - \frac{1}{2}\underline{q}\right)^2 \rho_0^2\, K_2\left(|\underline{k} - \frac{1}{2}\underline{q}|\rho_0\right)\right]^2 , \tag{47}$$

which naturally reduces to Eq. (23) when $\underline{q} = 0$. To obtain the slope of our pomeron we need to expand Eq. (47) up to the quadratic term in $\underline{q}^2$. After expansion of Eq. (47) in $\underline{q}^2$ and integration over the angles we obtain

$$I \;=\; I_0 \;+\; \pi\, \underline{q}^2\, \rho_0^2 \int_0^\infty dk\, \rho_0\; L(k\rho_0) \tag{48}$$

where

$$L(k\rho_0) \;=\; -\frac{1}{32(k\rho_0)^9}\left(1 - \frac{1}{2}(k\rho_0)^2 K_2(k\rho_0)\right)^2 \big[32 + (k\rho_0)^6 K_1(k\rho_0)^2 + 4(k\rho_0)^4 K_2(k\rho_0) + 8(k\rho_0)^4 K_2^2(k\rho_0)$$

$$-2(k\rho_0)^6 K_2^2(k\rho_0) + 2\,(k\rho_0)^4 K_0(k\rho_0)\left(1 - \frac{1}{2}(k\rho_0)^2 K_2(k\rho_0)\right) - 20(k\rho_0)^3 K_3(k\rho_0) + 2(k\rho_0)^5 K_2(k\rho_0) K_3(k\rho_0)$$

$$+(k\rho_0)^6 K_3^2(k\rho_0) + 2(k\rho_0)^3 K_1(k\rho_0)\left(-10 + (k\rho_0)^2 K_2(k\rho_0) + (k\rho_0)^3 K_3(k\rho_0)\right) + 2(k\rho_0)^4 K_4(k\rho_0)$$

$$-(k\rho_0)^6 K_2(k\rho_0) K_4(k\rho_0)\big] . \tag{49}$$

The integral in Eq. (48) is dominated by the small values of the argument, as could be seen from the behavior of the function $L(k\rho_0)$. We can expand the function $L(k\rho_0)$ of Eq. (49) to obtain

$$L(k\rho_0) \;\approx\; -\frac{1}{256\, k\, \rho_0} \tag{50}$$

when the argument is small. The full integral of Eq. (47) is convergent, whereas the integral in Eq. (48) seems to be divergent in the infrared. Therefore to regularize it after we plug Eq. (50) in it we have to use q as a lower cutoff and $1/\rho_0$ as an upper cutoff. The result yields

$$I \, = \, I_0 \, - \, \frac{\pi}{256} \, q^2 \, \rho_0^2 \, \ln \frac{1}{q\rho_0}. \tag{51}$$

Recalling that a pomeron trajectory is given in terms of its' intercept and slope by

$$\Delta(t) \, = \, \Delta \, + \, \alpha' \, t \tag{52}$$

and comparing (52) to Eq. (28) and Eq. (51) we can conclude that for our pomeron

$$\frac{\alpha'}{\Delta} \, = \, \frac{\pi \rho_0^2}{256 I_0} \, \ln \frac{1}{q\rho_0}. \tag{53}$$

Since there is still some q dependence left in Eq. (53) we conclude that our pomeron's trajectory is not quite linear in t and the notion of pomeron's slope is not very well defined for it. A similar result was obtained for the soft pomeron trajectory in [45] using Regge theory, which seemed to confirm experimental data of [46]. The conclusion of [45] was drawn out of two-pion exchange model of hadronic interactions. We can obtain a numerical estimate of the pomeron's slope of Eq. (53) by assuming that $\ln \frac{1}{q\rho_0} \, \sim \, 1$. Substituting the values of I_0 from Eq. (24) and $\rho_0 = 0.3 \, fm = 1.5 \, GeV^{-1}$ into Eq. (53) we obtain

$$\frac{\alpha'}{\Delta} \, \approx \, 2.0 \, GeV^{-2}, \tag{54}$$

which is remarkably close to the experimental result for the soft pomeron [41]

$$\left(\frac{\alpha'}{\Delta} \right)_{exp} \, = \, \frac{0.25}{0.08} \, GeV^{-2} \, \approx \, 3.1 \, GeV^{-2}. \tag{55}$$

In principle the integral of Eq. (47) substituted in the Eq. (28) (or either Eq. (32) or Eq. (36)) can give us the full trajectory of our pomeron. The integral in Eq. (47) could be estimated numerically for positive values of $\underline{q}^2$, which corresponds to the negative values of $t = -\underline{q}^2$. However, for positive t the integral in Eq. (47) has a singularity and if taken literally would be simply divergent. The resolution of this problem is the following: one should first perform the integration in Eq. (47) for negative t and then analytically continue the results into the region of positive t. This should be done analytically and the exact analytical treatment of the integral in Eq. (47) seems to be rather complicated. Instead we will use an approximation, which preserves all the main qualitative features features of the answer.

Using Eq. (42) in Eq. (47) and performing the integration over k yields the following expression

$$I(t) \, \approx \, \frac{\pi}{256} \, \left\{ 2 e^{t\rho_0^2/2} - e^{t\rho_0^2/4} - \frac{t\rho_0^2}{2} \left[2 \, Ei \left(\frac{t\rho_0^2}{2} \right) - Ei \left(\frac{t\rho_0^2}{4} \right) \right] \right\}. \tag{56}$$

We can check the quality of the approximation done to obtain Eq. (56) by comparing its' value for $t = 0$ with I_0 in Eq. (24). Eq. (56) gives

$$I(0) \, \approx \, \frac{\pi}{256} \, \approx \, 0.012, \tag{57}$$

which is very close to the exact value $I_0 = 0.014$ in Eq. (24). If we expand Eq. (56) for small t up to the terms linear in t we would exactly recover the expression for the slope of the trajectory given by Eq. (53)! Thus Eq. (56) provides us with a very good approximation of the integral in Eq. (47).

Our soft pomeron's trajectory could be obtained by substituting $I(t)$ from Eq. (56) into Eq. (36) instead of I_0. This gives

$$\Delta_{soft}(t) \, = \, \frac{\pi \, d^2}{(N_c^2 - 1)^2} \, \left(\frac{2\pi}{\alpha} \right)^{4N_c} \, e^{-\frac{4\pi}{\alpha}} \, \frac{(4\pi)^6}{\alpha^3} \, \frac{1}{81} \, \frac{E_{sph}^2 \, \rho_0^2}{6 \, e^2} \, \left[{}_2F_4 \left(\frac{9}{2}, \frac{9}{2}; 1, 2, \frac{11}{2}, \frac{11}{2}; \frac{\pi \, E_{sph}^4 \, \rho_0^4}{6 \, \alpha \, e^2} \right) - 1 \right]$$

$$\times \frac{\pi}{256}\left\{2e^{t\rho_0^2/2} - e^{t\rho_0^2/4} - \frac{t\rho_0^2}{2}\left[2\,Ei\left(\frac{t\rho_0^2}{2}\right) - Ei\left(\frac{t\rho_0^2}{4}\right)\right]\right\}. \tag{58}$$

After taking into consideration the virtual corrections and the quark contributions the answer for the pomeron's trajectory becomes

$$\Delta_P(t) \,=\, \delta\left[\prod_{q=u,d,s,\ldots} 1.3\,\left(m_q\,\rho_0 - \frac{2\pi^2}{3}\,(0|\bar{q}q|0)\,\rho_0^3\right)\right]^2 \Delta_{soft}(t), \tag{59}$$

where $\Delta_{soft}(t)$ is given by Eq. (58)

The soft pomeron's trajectory of Eq. (59) is depicted in Fig. 8. It is plotted for $\rho_0 = 0.3fm$, $E_{sph} = 2.4GeV$, $\delta = 0.31$ and $\alpha \approx 0.75$, i.e., the same values as were used for the estimates of the pomeron's intercept in Sect. IIIC.

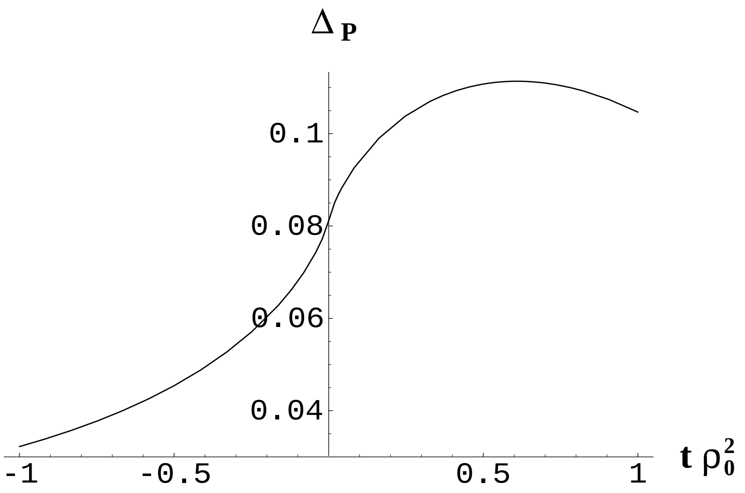

FIG. 8. Soft pomeron's trajectory. t is measured in the units of ρ_0^2.

As could be seen from Fig. 8 the soft pomeron's trajectory never becomes negative for negative t, which means that the total cross section generated by the soft pomeron exchange is always growing with energy. For positive values of t the trajectory first starts growing but then slows down and even turns over and falls off. It does not reproduce the linear growth behavior which would be predicted by Regge theory. However, the linear behavior of the trajectory for positive t is usually associated with confinement in QCD. It is a well known fact that the instanton–induced effects can not account for QCD confinement [3]. Therefore one should not expect that the pomeron constructed out of instantons should exhibit such confinement features as a linear trajectory for positive t. It is most likely that different non-perturbative physical mechanisms play an important rôle in that region.

V. SUMMARY AND DISCUSSION

In our approach we envision the soft pomeron as a chain of topological transitions induced by high momentum gluons. This is the main point of the paper. The corresponding pomeron ladder is depicted in Fig. 1. The multi–gluon vertices of the ladder are generated through a strong quasi–classical vacuum field.

To quantify the pomeron illustrated in Fig. 1 we have used the instanton fields, which have an explicit analytical form which we could employ. The resulting expressions for the pomeron intercept are given in Eqs. (32) and (36), corresponding to different ways of averaging over the instanton sizes. We have estimated the virtual corrections and showed that they are likely to change the value of the soft pomeron's intercept by a factor of $2 \div 3$ at the most. The numerical value of the intercept has been plotted in Fig.

6 as a function of the running coupling constant. The resulting intercept at $\alpha_s(1/\rho_0) = 0.7$ is very close to the phenomenological value of 0.08 [41]. The intercept falls off at small distances, which agrees with phenomenological observations of [41]. At short distances (small momenta) the dominant contribution to the structure functions comes from the hard pomeron [41]. The work on understanding how our soft pomeron merges with hard (BFKL) pomeron in that region is under way [47]. At large distances (small momenta) the pomeron's intercept also decreases. That way, in the region where the coupling constant is large and the interactions are very strong the pomeron's intercept can still be small. Thus our results could provide the resolution of the long-standing puzzle of the smallness of the soft pomeron intercept [41] in the strong coupling regime.

Finally, we have calculated the slope of the soft pomeron in Eq. (54). The value of the slope turned out to be close to the phenomenologically suggested value of 0.25 GeV^{-2} [41]. The full trajectory of the pomeron has also been derived (see Eq. (58) and Eq. (59)) and plotted in Fig. 8. Since the instantons can not account for confinement in QCD we do not expect a linear trajectory for positive t. For negative t, as the absolute value of t is getting larger the trajectory ceases to be linear and exhibits some curvature.

We can also estimate the multiplicity of the produced particles in a hadron–hadron scattering event mediated by our pomeron of Fig. 1. The particles would be produced by multiperipheral mechanism. From the estimate of Eq. (37) we can conclude that the density of instantons per unit of rapidity is rather small. However, since there are several particles emitted coherently from each instanton, we may expect correlations in particle production.

Let us estimate the typical number of particles produced on an instanton in the ladder of Fig. 1. For that purpose we will consider the series of Eq. (31) and estimate the average n in that series. That would be a typical multiplicity of gluons produced off an instanton. A simple calculation yields

$$\langle n \rangle \, = \, 1 + \frac{\pi \, E_{sph}^4 \, \rho_0^4}{6 \, \alpha_s e^2} \, \frac{{}_0F_2 \left(-; 2, 2; \frac{\pi E_{sph}^4 \, \rho_0^4}{6 \alpha_s e^2} \right)}{{}_0F_2 \left(-; 1, 1; \frac{\pi E_{sph}^4 \, \rho_0^4}{6 \alpha_s e^2} \right)}. \tag{60}$$

For the values of the parameter we have used above in estimating the pomeron's intercept, $E_{sph} = 2.4\,\mathrm{GeV}$, $\rho_0 = 0.3 fm$, $\alpha_s \approx 0.7$ (see Fig. 6), we obtain $\langle n \rangle \approx 3$. This result agrees with the estimate of [20].

While our numerical results are very sensitive to a number of instanton–related parameters, we believe that our approach can provide an interesting new insight in the mechanism of high–energy scattering and particle production in QCD. Further theoretical and experimental developments are clearly needed to clarify the relationship between the soft pomeron and the properties of the QCD vacuum.

ACKNOWLEDGMENTS

The authors are very much indebted to Ian Balitsky, Larry McLerran, Al Mueller and Edward Shuryak for numerous helpful discussions about instantons. We would like to thank James Bjorken, Greg Carter, Hirotsugu Fujii, Asher Gotsman, Lev Lipatov, Uri Maor, Rob Pisarski, Andreas Ringwald, Thomas Schäfer, Fridger Schrempp, Dam Son, Chung-I Tan, Arkady Vainshtein and Valentin Zakharov for many informative and encouraging discussions. Yu. K. would like to thank the High Energy Physics Department at Tel Aviv University for their support and hospitality during the final stages of this work. E. L. thanks BNL Nuclear Theory group for their hospitality and creative atmosphere during several stages of this work.

This manuscript has been authored under Contract No. DE-AC02-98CH10886 with the U. S. Department of Energy. The research of Yu. K. and E. L. was supported in part by the BSF grant # 9800276 and by Israeli Science Foundation, founded by the Israeli Academy of Science and Humanities.

[1] A. A. Belavin, A. M. Polyakov, A. A. Schwartz, and Y. S. Tyupkin, Phys. Lett. **B 59**, 85 (1975).
[2] G. 't Hooft, Phys. Rev. Lett. **37**, 8 (1976).

[3] C.G. Callan, R. Dashen, and D.J. Gross, Phys. Lett. **B63** 334, (1978); Phys. Rev. **D17** 2717, (1978).

[4] R. Jackiw and C. Rebbi, Phys. Rev. Lett. **37**, 172 (1976).

[5] E.V. Shuryak, Nucl. Phys. **B203**, 93, 116, 140 (1982).

[6] D. Diakonov and V. Petrov, Nucl. Phys. **B245**, 259 (1984).

[7] T. Schäfer, E. V. Shuryak, Rev. Mod. Phys. **70**, 323 (1998).

[8] J. D. Bjorken, Report No. hep-ph/9611421, and references therein.

[9] A. Ringwald, Nucl. Phys. **B330**, 1 (1990); O. Espinosa, Nucl. Phys. **B343**, 310 (1990).

[10] L. McLerran, A. Vainshtein and M. Voloshin, Phys. Rev. **D42**, 171, 180 (1990).

[11] P. G. Tinyakov, Int. J. Mod. Phys. **A8**, 1823 (1993); A. N. Kuznetsov and P. G. Tinyakov, Mod. Phys. Lett. **A11**,479 (1996).

[12] V. A. Rubakov, D. T. Son, and P. G. Tinyakov, Phys. Lett. **B287**, 342 (1992).

[13] A. H. Mueller, Nucl. Phys. **B348**, 310 (1991); Nucl. Phys. **B381**,597 (1992).

[14] For a review, see e.g. V.A. Rubakov and M.E. Shaposhnikov, Sov. Phys. Usp. **39** (1996) 461; hep-ph/9603208.

[15] I.I. Balitsky and V.M. Braun, Phys. Lett. **B314**, 237 (1993).

[16] A. Ringwald, F. Schrempp, Phys. Lett. **B459**,249 (1999) and references therein.

[17] I. Balitsky, M. Ryskin, Phys. Lett. **B 296**, 185 (1992).

[18] I. Balitsky, V. Braun, Nucl. Phys. **B380**, 51 (1992); Phys. Rev. D **47**, 1879 (1993).

[19] V. I. Zakharov, Nucl. Phys. **B383**, 218 (1992); **B371**, 637 (1992).

[20] D. Kharzeev and E. Levin, Nucl. Phys. **B 578**, 351 (2000).

[21] H. Fujii and D. Kharzeev, Phys. Rev. **D 60**, 114039 (1999); hep-ph/9807383.

[22] V. A. Novikov, M. A. Shifman, A. I. Vainshtein, and V. I. Zakharov, Nucl. Phys. **B191**, 301 (1981).

[23] D. Kharzeev, Yu. Kovchegov, E. Levin, in preparation.

[24] E.V. Shuryak, hep-ph/0001189.

[25] E. Shuryak and I. Zahed, hep-ph/0005152.

[26] E. Meggiolaro, Nucl. Phys. Supp. **B64**, 191 (1998).

[27] E.A. Kuraev, L.N. Lipatov and V.S. Fadin, *Sov. Phys. JETP* **45**, 199 (1978).

[28] Ya.Ya. Balitsky and L.N. Lipatov, *Sov. J. Nucl. Phys.* **28**, 22 (1978).

[29] Ya. Balitsky, D. Kharzeev, Yu. Kovchegov, E. Levin, in preparation.

[30] A.H. Mueller, Nucl. Phys. **B415**, 373 (1994); A.H. Mueller and B. Patel, Nucl. Phys. **B425**, 471 (1994); A.H. Mueller, Nucl. Phys. **B437**, 107 (1995); Z. Chen, A.H. Mueller, Nucl. Phys. **B451**, 579 (1995).

[31] E.V. Shuryak, Nucl. Phys. **B203**, 93 (1982).

[32] Yu. V. Kovchegov, Phys. Rev. D **60**, 034008 (1999); Yu. Kovchegov, E. Levin, Nucl. Phys. **B577**, 221 (2000).

[33] L. McLerran, E. Mottola, M. Shaposhnikov, Phys. Rev. D **43**, 2027 (1991).

[34] D. Amati, S. Fubini and A. Stanghelini, Nuovo Cimento **26** (1962) 896;
Yu. P. Nikitin and I.L. Rosental, *“ Theory of Multiparticle Production Processes”*, Harwood Academic, 1988;
“Hadronic Multiparticle Production”, ed. P. Carruthers, World Scientific, 1988;
The collection of the best original papers on Reggeon approach can be found in:
“ Regge Theory of low p_t Hadronic Interaction”, ed. L. Caneschi, North - Holland, 1989;
A. Capella, U. Sukhatme, C-I Tan, J. Tran Thanh Van, Phys. Rept. **236**, 225 (1994).

[35] Yu. L. Dokshitzer, *High Energy Physics*, vol. 1, pp. 305-324, Vancouver 1998 (Report No. hep-ph/9812252) and references therein.

[36] V. N. Gribov, Eur. Phys. J. **C10**, 71 (1999); **C10**, 91 (1999).

[37] L. V. Gribov, E. M. Levin, and M. G. Ryskin, Phys. Rep. **100**, 1 (1983).

[38] M. A. Shifman, A. I. Vainshtein, V. I. Zakharov, Phys. Lett. **76B**, 471 (1978).

[39] D. Diakonov, M. Polyakov, C. Weiss, Nucl. Phys. **B461**,539 (1996).

[40] G. ’t Hooft, Phys. Rev. **D 14**, 3432 (1976); C. W. Bernard, N. H. Christ, A. H. Guth, and E. J. Weinberg, Phys. Rev. **D 16**, 2967 (1977); L. S. Brown, and D. B. Creamer, Phys. Rev. **D 18**, 3695 (1978); A. I. Vainshtein, V. I. Zakharov, V. A. Novikov, and M. A. Shifman, Sov. Phys. Usp. **25**, 195 (1982).

[41] A. Donnachie, P. V. Landshoff, Phys. Lett. **B296**, 227 (1992); Phys. Lett. **B437**, 408 (1998) and references therein.

[42] J. W. Negele, Nucl. Phys. Proc. Suppl. **73**, 92 (1999).

[43] E. V. Shuryak, Phys. Rev. **D52**, 5370 (1995).

[44] M. A. Shifman, A. I. Vainshtein, V. I. Zakharov, Nucl. Phys. **B165**, 45 (1980); **B163**, 46 (1980).

[45] A. A. Anselm, and V. N. Gribov, Phys. Lett. **B 40**, 487 (1971).

[46] M. Holder et al., Phys. Lett. **B 36**, 400 (1971) and references therein.

[47] D. Kharzeev, Yu. Kovchegov, E. Levin, C.-I. Tan, K. Tuchin, in preparation.